

Effects of pulsed hollow electron lens operation on the beam core in HL-LHC: First experimental studies and simulations.*

Miriam Fitterer,[†] Giulio Stancari, and Alexander Valishev
Fermi National Accelerator Laboratory, Batavia, Illinois, USA

Stefano Redaelli and Daniel Valuch

CERN, Geneva, Switzerland

(Dated: January 29, 2018)

In case of the High Luminosity Large Hadron Collider (HL-LHC), a considerable amount of energy is stored in the beam tails due to the high beam intensity and, in addition, an overpopulation of the tails compared to a Gaussian distribution. To control and clean the tail population, the installation of two hollow electron lenses, one per beam, is foreseen. Beside the DC operation of the lenses, also pulsed operation is considered having the advantage to considerably increase the diffusion speed by exerting noise on the halo particles. In the ideal case, that is in case of no field at the proton beam core, only the halo particles are excited while leaving the core unperturbed. The picture though changes, if a residual field is present also at the location of the beam core exposing also the particles in the center to noise. In this paper, we present first estimates of the residual field at the proton beam core expected from the HL-LHC hollow electron lens and summarize the results of the LHC experiments conducted in 2016 and 2017 to study the effects on the beam core in case of pulsed operation.

I. INTRODUCTION

Considering past, current and future high energy and intensity colliders, each new machine has represented a considerable leap in stored beam energy with rising values for future accelerators and colliders (see Table I). Recent measurements at the LHC furthermore show that the tails of the transverse beam distribution are overpopulated compared to a Gaussian distribution resulting in a considerable amount of energy being stored in the beam tails alone. In case of the LHC explicitly around 5% of the beam population is stored in the tails above 3.5σ compared to 0.22% in case of a Gaussian distribution leading to 19 MJ of stored energy in the tails in case of nominal LHC parameters and 34 MJ in case of HL-LHC [6].

All of the above reasons lead to the conclusion that a mechanism is needed to deplete the beam tails in a controlled manner [7]. The most obvious idea is to decrease the collimator gaps or scrape the tails with a collimator type device. The minimum gap size of the collimators is however limited by the impedance of the machine. Small enough gap sizes can therefore not be reached without risking severe beam instabilities. Other mechanisms must therefore be found to actively deplete the tails. Most promising are methods, which increase the diffusion speed in the region of the halo particles while

leaving the beam core unperturbed. The diffusing halo particles are then intercepted by the collimation system and removed. This concept is also referred to as active halo control compared to a passive system, which only intercepts the halo particles without actively controlling the diffusion speed (see Fig. 1 for illustration).

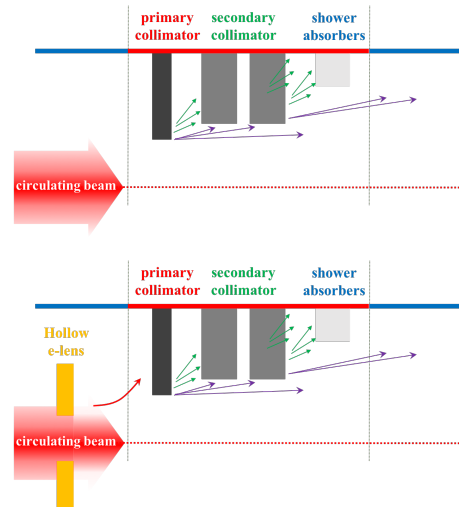


FIG. 1. Sketch of passive halo control as with the collimation system (top) and active halo control using in addition for example a hollow electron lens (HEL) to control the diffusion speed in the region tail region without affected the beam core (bottom).

* Fermilab is operated by Fermi Research Alliance, LLC under Contract No. DE-AC02-07CH11359 with the United States Department of Energy. This work was partially supported by the US DOE LHC Accelerator Research Program (LARP) and by the European FP7 HiLumi LHC Design Study, Grant Agreement 284404.

[†] mfittere@fnal.gov

In a recent review, the need for such an active halo control system for HL-LHC has been assessed with the conclusion that it would considerably increase the margin and reduce the risk for machine protection compared to the current LHC collimation system being a passive halo control system [7]. In view of the general need of active

TABLE I. Stored beam energy for different past, present and future colliders. Each new machine represents a leap in stored beam energy.

Collider	Tevatron (protons) [1]	LHC 2016 [2]	LHC nominal [3]	HL-LHC [4]	FCC [5]
Beam energy [TeV]	0.98	6.5	7.0	7.0	50.0
Number of bunches	36	2220	2808	2748	?
Number of particles per bunch	2.90×10^{11}	1.15×10^{11}	1.15×10^{11}	2.2×10^{11}	1.0×10^{11}
Stored beam energy [MJ]	1.6	265.9	362.2	678.0	8400

halo control for future high power accelerators and HL-LHC in particular, different methods have been studied in the last recent years [8], of which the HEL is considered the superior device at least in case of the HL-LHC [7] and is also considered for other future high energy colliders like HE-LHC and FCC-hh [9, 10].

The beneficial effect of an active halo control system is however abrogated if also the beam core is affected as this would ultimately lead to a degradation of the performance due to losses of particles in the core region and emittance growth. In this paper, we will concentrate on this aspect in view of future HEL to be installed in the HL-LHC. We will summarize possible sources of perturbations of the beam core concentrating in particular on the case of pulsed operation and with the focus on the beam experiments at the LHC performed in this context.

This paper is structured as follows: Section II gives an introduction to the concept of HELs and summarizes the design parameters of the HL-LHC HEL. Section III is dedicated to describing the sources of a residual field from the HEL in the core region. Section IV describes then in detail the two beam experiments conducted at the LHC to study the effect on the beam core in case of a pulsed HEL operation. This includes the detailed analysis of the observed losses, emittance and transverse beam distribution changes. To the knowledge of the authors, the observed distribution changes presented in this paper have never been measured before in the context of a resonant excitation. A resonant excitation has been previously studied at the Tevatron in the context of the HEL experiments [11] and the abort gap cleaning used in operation [12]. Both studies however only concentrated on the losses and emittance changes without measuring the detailed changes of the distribution itself. In addition, the presented experiments also provide scalings of the losses and emittance growth with the excitation amplitude. This allows to provide first tolerances for the residual field of the HL-LHC HEL at the beam core and also to compare the obtained results with simulations and thus benchmark the same.

II. HOLLOW ELECTRON LENS FOR HL-LHC

A. General Overview

In general, electron lenses are DC or pulsed low energy electron beams. The electron beam is generated

in an electron gun, then guided and confined by strong solenoids and finally dumped onto a collector. Exemplary for the conceptual design of all electron lenses, the HL-LHC HEL is shown in Fig. 2. The circulating beam, in

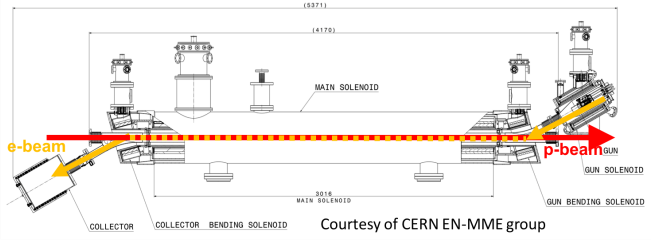


FIG. 2. Layout of HL-LHC HEL.

case of the LHC the proton beam, is then affected by the electromagnetic field of the electron beam. For the application of active halo control, the electron beam needs to generate an electromagnetic field at the location of the halo particles while leaving the core untouched. This can be achieved by using a uniform hollow distribution in radius $r = \sqrt{x^2 + y^2}$ with inner radius R_1 and outer radius R_2 . In this case, the circulating proton beam experiences a radial kick $\theta(r)$

$$\theta(r) = \frac{f(r)}{(r/R_2)} \cdot \theta_{\max}, \quad (1)$$

where $f(r)$ is a shape function with

$$f(r) = \begin{cases} 0 & , \quad r < R_1, \\ \frac{r^2 - R_1^2}{R_2^2 - R_1^2} & , \quad R_1 \leq r < R_2, \\ 1 & , \quad R_2 \leq r \end{cases} \quad (2)$$

and $\theta_{\max} = \theta(R_2)$ is the maximum kick angle given by

$$\theta_{\max} = \theta(R_2) = \frac{2LI_T(1 \pm \beta_e \beta_p)}{4\pi\epsilon_0 \cdot \left(\frac{q}{p_0}\right)_p \cdot \beta_e \beta_p c^2} \cdot \frac{1}{R_2}, \quad (3)$$

where L is the length of the e-lens, I_T the total electron beam current, β_e and β_p the relativistic β of electron and proton beam, $\frac{q}{p_0} = (B\rho)_p$ the magnetic rigidity for the reference particle, c the speed of light and ϵ_0 the vacuum permittivity.

The distribution together with the resulting kick are illustrated in Fig. 3. The \pm -sign represents the two cases

TABLE II. HL-LHC hollow electron lens parameters as in [13].

Geometry	Value	Unit
Length L	3	m
Desired range of scraping positions ^a	4-8	σ_p
Magnetic fields		
Gun solenoid, B_g	0.2-0.4	T
Main solenoid, B_m	2-6	T
Collector solenoid, B_c	0.2-0.4	T
Compression factor ($k = \sqrt{B_m/B_g}$)	2.2-5.5	-
Electron gun		
Peak yield I_e at 10 keV	5.0	A
Gun perveance P	5	μperv
Inner/outer cathode radius, R_1/R_2	6.75/12.7	mm
High voltage modulator		
Cathode-anode voltage	10.0	kV
Rise time (10%-90%)	200	ns
Repetition rate	35	kHz

^a σ denotes here the Beam sigma and not the collimation σ which assumes a normalized emittance of 3.5 μm .

of the electron beam traveling in the direction of the proton beam ($v_e v_p > 0$) leading to “−” or in the opposite direction ($v_e v_p < 0$) leading to “+”. For hollow electron beam collimation, electron and proton beam travel in opposite directions. Assuming HL-LHC and HEL design parameters (Table II–III) the maximum kick of the HEL is:

$$\theta_{\max, \text{B1}} = 392 \text{ nrad} \quad (4)$$

for an inner radius $R_1 = 4\sigma_p$, outer radius $R_2 = 7.5\sigma_p$ and a peak current of $I_e = 5.0 \text{ A}$. Similar values are obtained for Beam 2.

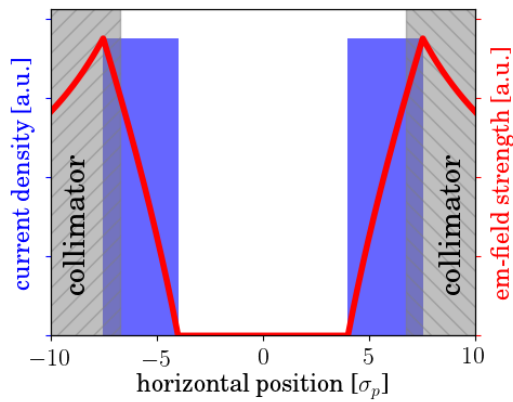


FIG. 3. Illustration of the hollow electron beam distribution (blue), the kick experienced by the proton beam (red) and the collimators (gray).

TABLE III. HL-LHC design parameters at top energy [4] and parameters relevant in connection with the HEL. Optics parameters at HEL are based on a position of the HEL of −40 m for Beam 1 (B1) and +40 m for Beam 2 (B2) from IP4 using HL-LHC optics V1.3 with $\beta^* = 0.15 \text{ m}$ [16].

Beam parameters	Value(B1)	Value(B2)	Unit
Beam energy E_p	7	TeV	
Number of bunches n_b	2748	-	
Number of particles per bunch N_b	2.2×10^{11}	-	
Normalized emittance $\epsilon_{N,x/y}$	2.5	μm	
Bunch spacing	25	ns	
Optics parameters at HEL (Beam 1) ^a			
β_x at HEL	197.5	280.6	m
β_y at HEL	211.9	262.6	m
Dispersion D_x at HEL	0.0	0.0	m
Dispersion D_y at HEL	0.0	0.0	m
Proton beam size $\sigma_{p,x}$ at HEL	0.26	0.31	mm
Proton beam size $\sigma_{p,y}$ at HEL	0.27	0.30	mm
scraping position $\sigma_p = \max(\sigma_{p,x}, \sigma_{p,y})$	0.27	0.31	mm

^a As the twiss parameters at IP4 do not change during the entire squeeze, and IP4 and the HEL are only separated by a drift space, the twiss parameters stay constant also at the HEL during the entire squeeze.

B. Operation modes and effects on the beam core

As depicted in Fig. 3 and in evidence from Eq. 1–2, the field at the beam core vanishes in the ideal case. Effects on the beam core thus only arise in case of imperfections, where possible sources are the bends of the HEL, as the electron beam crosses directly the proton beam, and distortions in the electron beam profile (see Section III). Both sources result in non-linear kicks [14, 15].

In DC operation of the HEL, these non-linear kicks stay in the shadow of the non-linearities otherwise present in the machine. Tolerances on imperfections are therefore not particularly stringent and of no concern.

The picture changes significantly in case of pulsed operation of the HEL, in which case the electron gun voltage is modulated using a white or colored noise spectrum. If the electromagnetic field of the HEL does not vanish at the proton beam core, noise is transferred not only to the halo particles, as intended, but also to the beam core with naturally much smaller amplitude. Tolerances in this case rapidly become much more stringent than in the case of DC operation and studies of the effect of the HEL on the beam core are therefore focusing on this mode of operation which is also the main topic of this paper.

Despite the fact that pulsed operation is much more dangerous than DC operation for the proton beam core, pulsed operation is still strongly under consideration. The main benefit of pulsing the HEL is to increase the halo removal rate if a fast depletion of the halo is desired. The halo diffusion rate is increased in this case as in addition to the non-linear kick, noise is exerted on the

halo particles of the proton beam. For the HL-LHC two different pulsing patterns are considered:

- **random excitation:** The electron gun voltage is modulated between:

$$U_{\text{e-gun}} = a \cdot U_{\text{max}} \quad (5)$$

$$+ (1 - a) \cdot \text{ran}(0, 1) \cdot U_{\text{max}} \quad (6)$$

with U_{max} the equivalent voltage in DC operation, a the modulation strength with $a \in [0, 1]$, and $\text{ran}(0, 1)$ a uniformly distributed random number between $[0, 1]$.

- **resonant excitation:** The HEL is switched on only every k^{th} turn. The excitation can then be represented by:

$$f(t) = \sum_{p=-\infty}^{+\infty} \delta(t - n \cdot (kT)), \quad (7)$$

where p is the turn number and T the revolution time, and its Fourier series by:

$$f(t) = \text{III}_{kT}(t) = \frac{1}{kT} \sum_{n=-\infty}^{+\infty} e^{2\pi i f_n t} \quad (8)$$

$$\text{with } f_n = \frac{n}{k} f_{\text{rev}}, \quad (9)$$

where III_{kT} is the Dirac comb. As can be seen from the Fourier series, k^{th} turn pulsing in general drives k^{th} order resonances [17]. Historically, the k^{th} turn pulsing was used in regular operation in the Tevatron for abort cleaning [12].

In general, the random excitation mode is the most effective and operationally easiest pulsing mode, but also the most stringent in terms of tolerances on the residual field at the beam core as it induces white noise and thus excites all beam frequencies. As the resonant excitation acts on specific resonances, the pulsing pattern has to be chosen according to the machine and beam parameters. On the one hand, this makes the operation more difficult as one has to find the most efficient k^{th} turn pulsing for each operation mode, on the other hand, it also relaxes the tolerances on the residual field at the beam core as, depending on the machine and beam configuration, it might be possible to find a resonant excitation pattern, which mainly affects the halo and not the core.

III. SOURCES OF RESIDUAL FIELD IN THE PROTON BEAM CORE REGION AND FIRST ORDER ESTIMATES

With the current HEL layout (see Fig. 2), parasitic kicks on the proton beam core can arise in the central region (main solenoid) due to profile imperfections in the

electron beam and at the entrance and exit of the HEL, where electron and proton beam overlap. Currently, no HEL is installed in the LHC, and the kick on the proton beam core must therefore be approximated to first order by a dipole kick for the experiments at the LHC. During the experiments presented in this paper, the dipole kick with the corresponding excitation pattern was applied with the LHC transverse damper (see Section IV B).

Leaping ahead of the more detailed derivations in Sec. III A and Sec. III B, the expected kick to first order from the HEL bends is estimated to be (Eqn. 14):

$$\Delta x'_{\text{bends}}, \Delta y'_{\text{bends}} \leq 0.5 \text{ nrad}, \quad (10)$$

and for the central region due to profile imperfections (Eqn. ??):

$$\Delta x'_{\text{central region}}, \Delta y'_{\text{central region}} \leq 19.6 \text{ nrad} \quad (11)$$

where the current HEL design parameters (see Table III–II) are used. The contribution from the central region is clearly dominating.

A. Uncompensated kicks from HEL bends

As reference for the estimate of the dipole component originating from the HEL bends, the symplectic map derived in [14] is used. In this case the HEL bends are modeled as a cylindrical pipe with a static charge distribution of 1 A and 5 keV electrons bend in the horizontal plane. In case of an U-shaped HEL, the transverse dipole kicks at entrance and exit add up, while for a S-shaped HEL the kicks compensated each other. For this reason a S-shape has been chosen for the HL-LHC HEL (see Fig. 2). In this case, uncompensated kicks therefore only arise from imperfections, which can originate from profile imperfections and current fluctuations. As a first rough estimate, we assume in this paper 10% fluctuations between the entrance and exit and that the kicks from entrance and exit due to these imperfections add up. Using the electric field calculations in [14], the maximum values for the integrated electric field are then around

$$\int_{z_1}^{z_2} E_{x,y} dz = 10 \text{ kV} \quad (12)$$

assuming an 1 A, 5 keV electron beam. Neglecting magnetic effects and scaling to HL-LHC and HEL design parameters (Table II–III) this yields a kick of:

$$\int_{z_1}^{z_2} E_x dz = 36 \text{ kV} \Rightarrow \Delta x' = 5.1 \text{ nrad} \quad (13)$$

Assuming now 10% fluctuation between entrance and exit kick, the expected kick from the HEL bends is

$$\Delta x', \Delta y' = 0.5 \text{ nrad}. \quad (14)$$

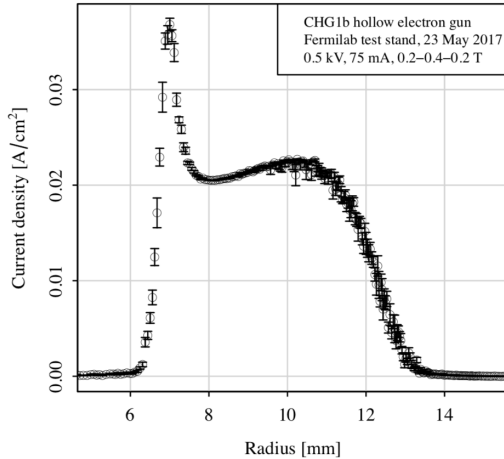


FIG. 4. Current density from measurements of the CHG1b hollow electron gun at the Fermilab electron lens test stand in 2017 [19].

B. Kicks in the central region (main solenoid)

For a perfectly uniform, annular and radially symmetric profile, the field in the region of the proton beam core vanishes (see Eqn. 2 and Fig. 3). Fields at the location of the proton beam core, thus only arise in case of profile imperfections of the electron beam, in particular if the radial symmetry is broken.

Last year, new measurements could be performed at the Fermilab electron lens test stand [18] of the newest hollow electron gun CHG1b. A typical measurement of the electron beam current density obtained during these measurements is shown in Fig. 4. As at the test stand the solenoidal fields required for the HL-LHC electron lens can not be reached, an estimate of the electron beam profile for HL-LHC can only be obtained in terms of simulations. For this purpose, the measured distribution is compressed to the inner e-beam radius of 0.97 mm and than an input distribution with 40 000 particles generated. The electric field can in general be scaled with the electron beam current and energy, but can not easily be scaled with the inner and outer radius of the electron beam distribution. Therefore it is essential to track a distribution with the correct dimensions. The potential and fields can then be calculated with the particle in cell simulation code WARP [20] yielding the relative electric field strengths shown in Fig. 5. Further details on the measurements and WARP simulations can be found in [19].

As a first estimate for the fields at the proton beam core, one can use the relative electric field strength along the x- and y-axis, yielding roughly (Fig. 5, right):

$$E_{\text{rel}} \approx 5\% \quad (15)$$

For a maximum kick of 392 nrad (Eqn. 4), we then obtain as estimated dipole kick amplitude at the proton beam

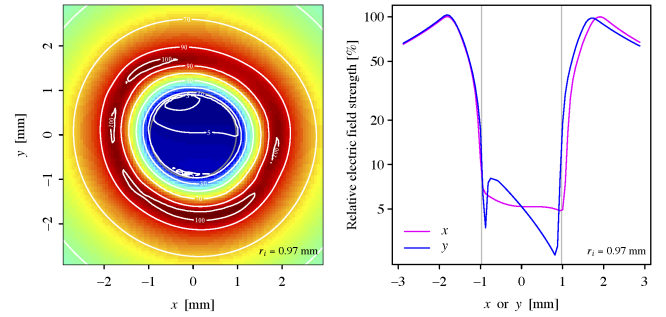


FIG. 5. Calculated relative electric field for the new CHG1b hollow electron gun in the x-y plane and as projection on the x- and y-axis respectively based on measurements at the Fermilab test stand combined with WARP simulations for the calculation of the electric potentials and fields.

core:

$$\Delta x'_{\text{central region}}, \Delta y'_{\text{central region}} \leq 19.6 \text{ nrad} \quad (16)$$

IV. LHC EXPERIMENTS

A. Overview of LHC experiments

The experiments at the LHC presented in this paper were aiming at deriving tolerances on the residual HEL field at the location of the beam core in case of pulsed operation. In total, two experiments were conducted, the first one in 2016 [21] and the second one in 2017 [22]. The beam and machine parameters for both experiments are summarized in Table IV. As there is currently no HEL installed in the LHC, the kick on the beam core is emulated by a dipole kick applied with the transverse damper of which more details are given in Section IV B. Explicitly, all orders higher than the first order are neglected. Preceding the beam experiments, simulations were performed to identify the most effective pulsing pattern for the k^{th} turn pulsing (see Sec. IV D 1) and yield estimates for losses and emittance growth. The two k^{th} turn pulsing patterns with the largest effect, one k^{th} turn pulsing pattern with no effect and the random excitation could then be experimentally tested in the LHC limited obviously by the beam time available. To at least test the reproducibility of the results on the example of one pulsing pattern, the 7th turn turn pulsing was tested in the 2016 experiments and then repeated in the 2017. During the experiments the losses were measured with the fast beam current transformers (FBCT) and the emittance and transverse beam profiles with the beam synchrotron radiation telescope (BSRT). The analysis of the BSRT profiles is quite involved and we therefore concentrate in this paper only on the main results. A detailed description of the analysis can be found in [23] and for the individual experiments in [21, 22].

TABLE IV. Beam parameters and machine configuration as used in the two resonant excitation experiments in 2016 and 2017 [21, 22]. The plane of the excitation is abbreviated with H for horizontal, V for vertical and H+V horizontal and vertical at the same time.

Parameter	Experiment 2017	Experiment 2016
beam	Beam 1	
beam energy	injection energy, 450 GeV	
single bunch intensity	0.7×10^{11}	
normalized emittance	$2.5 - 3.5 \mu\text{m}$	
4σ bunch length	1.3 ns	
1σ bunch length	9.7 cm	
number of bunches	$3 \times 72 = 216$ bunches (+ 1 pilot + 12 nominal)	$12 \times 4 = 48$ single bunches
injection optics, $\beta^* = 11$ m	standard optics 2017	standard optics 2016
Landau damping octupoles	$I_{\text{MO}} = \pm 19.6$ A, explicitly +19.6 A for MOF circuit and -19.6 A for MOD circuit (standard 2016 settings)	
working point (Q_x, Q_y)	(62.27,60.295)	(64.28,59.31)
chromaticity (Q'_x, Q'_y)	(+15,+15)	
pulsing patterns	7 th turn H,V,H+V; 8 th turn H,V,H+V; random H,V,H+V;	7 th turn H; 10 th turn V;

B. Excitation with transverse damper and filling scheme

The primary function of the transverse feedback system in LHC, also referenced to as ADT, is to provide injection oscillation damping and actively damp the coupled bunch instabilities driven by the machine impedance. The main building blocks of the ADT system are stripline pickups at the position Q7 and Q9 at Point 4 of the LHC, connected to the beam position measurement modules at the surface, the digital signal processing modules (mDSPU) and a set of tetrode power amplifiers feeding electrostatic kickers in the RF zone of the LHC [24, 25].

Though originally designed to damp the undesired transverse activities only, the damper is being routinely used for sophisticated beam excitations as well (e.g. Abort gap and injection gap cleaning, single bunch excitation for tune and linear coupling measurements, machine development etc.) thanks to the state of the art digital signal processing hardware.

The transverse feedback is in general active during the whole LHC cycle, therefore it is of very high importance, that the noise introduced by the system does not contribute to any emittance growth. The typical machine cycle requires a short damping time of 10-20 turns (high feedback gain) for injection oscillation damping, which is increased during the ramp and stable beams to 50-100 turns (lower feedback gain). It has been demonstrated that noise introduced by the transverse feedback system itself is sufficiently low to introduce any measurable emittance growth [26]. All excitation signals referenced to in this paper, are digitally synthesized in the damper's digital signal processing units and therefore can be considered as "noise-free".

The resonant excitation experiment in 2017 involved si-

multaneous measurements on three groups of 72 bunches with a dedicated excitation pattern and transverse feedback configuration on each sub-group of 6 bunches. In 2016 a similar configuration was used, but with only 48 bunches in total. Both schemes are illustrated in Fig. 6.

The excitation in the horizontal and the vertical plane is generated by a different set of signal processing hardware, however during this experiment the signals were synchronized at a turn level. This means the bunches of the third group (of 72 bunches) experienced the kick in both horizontal and vertical plane during the same turn.

The ADT kicker deflection angle is calculated from the kicker geometry and the excitation voltage on the deflection plates. The excitation voltage used in the experiments is a complicated waveform, generated by a very complex hardware (digital signal processor, chain of transmission lines, low and high power amplifiers). The peak excitation voltage (and subsequently the kick) seen by the beam can be only indirectly measured using the probes on each kicker. The measured values are therefore believed to be known with an error margin of 10-15% for the experiments in 2017 and 50% in 2016. The error for 2016 is much larger as no calibration of the ADT was performed beforehand, which was done in 2017. As an example Fig. 7 shows the oscillation amplitude of each bunch in both H and V planes captured by the LHC real time transverse activity monitor. The measured activity is well in line with the expected excitation pattern.

C. Overview of simulations

For the preparation and interpretation of the experiments two different types of simulations were performed:

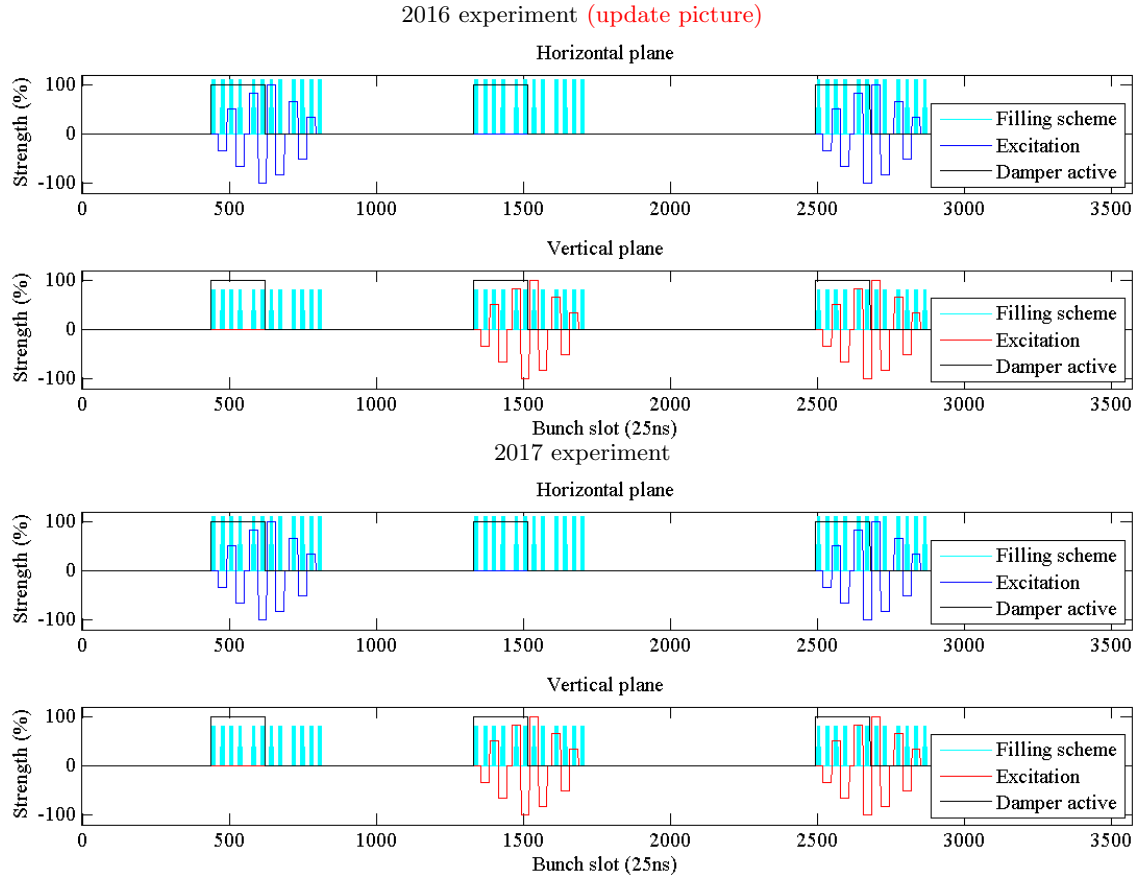


FIG. 6. Filling and excitation scheme for LHC experiments in 2016 (top) and 2017 (bottom).

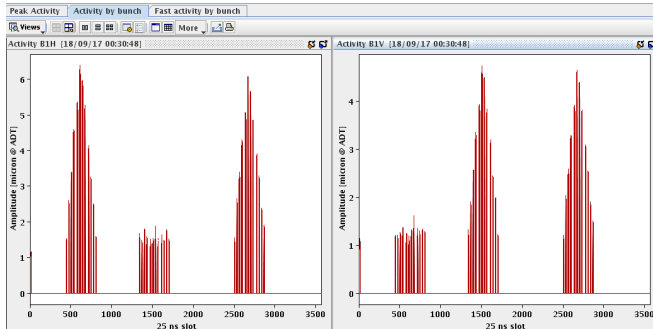


FIG. 7. Bunch by bunch excitation detected by the real time transverse activity monitor during the 2017 experiment (8th turn pulsing)

1. tracking of a Gaussian distribution (Distribution Tracking) to obtain loss rates and emittance growth,
2. Frequency map analysis (FMA) [27] for the visualization of resonances.

For both simulation types, the tracking code Lifetrac [28] was used. The simulation parameters are summarized in Table V. Further details on the simulations can be found in [17, 22].

D. Simulation and experimental results

In the following we will summarize the simulation and experimental results. We will jump forth and back between both as the experimental results are best understood on the base of the simulations. In summary, the most efficient pulsing patterns could be successfully predicted in simulations (Sec. IV D 1). Quantitative predictions of loss rates and emittance growth proved however challenging as both observables are influenced in addition by the natural noise present in the LHC originating for example from ground motion and magnetic field ripple. The observed effect is then the result of the interaction of the external excitation with the natural noise. At injection, this natural noise component is not known for the LHC. Beside the natural noise, also collective effects like intra-beam scattering and electron cloud influence the time evolution of emittance and losses. Both are not taken into account in the simulations.

The general dynamics of a resonant excitation seen in simulations is a fast adjustment to a new equilibrium distribution. In the presence of only a resonant excitation, this distribution is stable with a constant emittance as shown for example in Figs. 8 and 13. If the resonant excitation interacts with the natural noise sources, the beam distribution still changes to a new equilibrium dis-

tribution but this change is also accompanied by a resonant excitation amplitude dependent emittance growth as seen for example in Figs. 13, 16 and 19, and also observed experimentally, see for example Figs. 11 and 17. An excitation with random uniform noise on the other hand results in constant emittance growth without any initial adjustment phase. The interaction with the natural noise source then only manifests itself in an underestimation of loss rates and emittance growth. This is visible in simulations, see Fig. 23 as well as experimentally, see Fig. 24. The effect of a random excitation was also studied in more detail in [29, 30] for colliding beams at the LHC.

1. Prediction of the most efficient pulsing pattern

The most efficient pulsing pattern can be predicted by the comparison of the loss rate and emittance growth from the Distribution Tracking for the different pulsing patterns. As an example, the simulation results for the 2016 experiment are shown in Fig. 8 featuring a clear dependence of both parameters on the pulsing pattern. The largest losses are observed for 3rd, 7th and 10th turn pulsing and a uniform random excitation. As the bunch length decreases in accordance with the losses, the losses can be mostly associated to off-momentum particles. Only for 7th and 10th turn pulsing as well as for a random excitation considerable emittance growth is visible.

TABLE V. Summary of simulation parameters for the Distribution Tracking and FMA analysis. For details see [17, 22].

Parameter	Distribution Tracking	FMA
beam	Beam 1	
beam energy	450 GeV	
emittance	3.5 μm	2.5 μm
4 σ bunch length	1.3 ns	
1 σ bunch length	9.7 cm	
particle distribution	6D Gaussian distribution (10^4 particles)	equally spaced grid in x, y up to 10 σ with $\frac{\Delta p}{p_0} = 0$
turns tracked	10^6 turns	10^4 turns
optics	2016 or 2017 injection optics, $\beta^* = 11$ m	
machine imperfections	standard errors with $a_1 = b_1 = 0^a$	no errors
octupoles	$I_{\text{MOF}} = +19.6$ A, $I_{\text{MOD}} = -19.6$ A	
tune (Q_x, Q_y)	(64.28, 59.31) for 2016, (62.27, 60.295) for 2017	
chromaticity (Q'_x, Q'_y)	(+15, +15)	
transv. aperture	5.7 σ	-
long. aperture	10 σ	-

^a Orbit errors are disabled due to different implementation of the a_1, b_1 errors in Lifetrac and MAD-X. b_2 errors are adjusted to yield an average (over 60 seeds) peak β -beat of 15% as expected from optics measurements in the LHC.

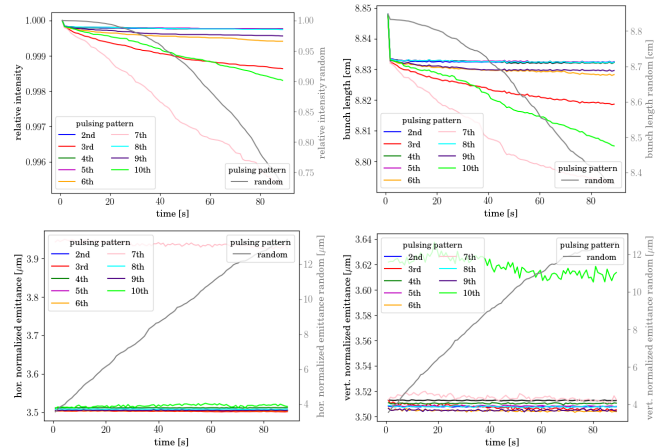


FIG. 8. Relative intensity (top left), bunch length (top right) and horizontal (bottom left) and vertical (bottom right) emittance obtained from simulation results (Distribution Tracking) for different pulsing patterns based on the 2016 injection optics with $(Q_x, Q_y) = (64.28, 59.31)$ with standard errors. The resonant excitation is applied in both planes with an amplitude of 96 nrad. No random noise component is added.

Compared to any k^{th} turn pulsing pattern, the random excitation has by far the strongest effect. The sensitivity to 7th and 10th turn pulsing is also observed in absence of machine errors in which case the only source of non-linearities are the strong sextupoles and octupoles [17]. This suggests that latter are the source of non-linearity responsible for this sensitivity. The driven resonances are revealed by the FMA analysis shown in Fig. 9. The $7Q_x$ resonance is excited in case of the 7th turn pulsing and the $10Q_x$ and $10Q_y$ resonance in case of the 10th turn pulsing for an excitation in both planes. As octupoles can only drive even resonances, the source of the $7Q_x$ resonances are the sextupoles while the octupoles only generate the tune footprint. The other pulsing patterns do not exhibit any increase in losses or emittance growth without magnetic errors and their effect thus is based on the magnetic field errors assigned, explicitly also the seed chosen for the simulation.

As already addressed earlier, the emittance in case of the 7th and 10th turn pulsing starts at an increased initial value and then stays almost constant during the entire simulation time. This behavior is typical for any k^{th} turn pulsing and can be ascribed to the adjustment of the beam distribution during the first 10^4 turns to a new equilibrium distribution. As the beam distribution is only dumped every 10^4 turns, this initial fast adjustment manifests itself in an increased initial emittance value in Fig. 8, and also any other simulations over 10^6 turns presented in this paper. Besides an increased emittance, the new distribution also becomes non-Gaussian. This can be seen by means of the residual in respect to the Gaussian distribution illustrated for example for the 7th and 10th turn pulsing in Fig. 10. For the purpose of comparison, also the distribution in both planes for a random

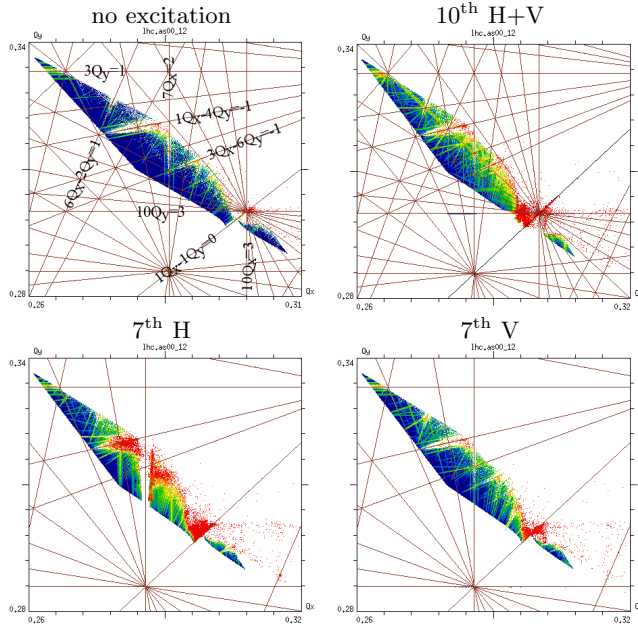


FIG. 9. FMA analysis for 7th and 10th turn pulsing based on the 2016 injection optics with no machine errors and a tune of (64.28,59.31). The excitation is 120 nrad in the corresponding plane. The absence of a strong excitation of any resonance in case of 7th turn pulsing only in V and the strong excitation in case of pulsing only in H further confirms that the 7Q_x resonance is the main resonance driven. For 10th turn pulsing there is in contrast no significant difference between pulsing only in H, only in V or in H+V (see Appendix A, Fig. 28).

excitation is shown. This initial fast change of the beam distribution is not only an artifact of the simulation, but has been, to the knowledge of the authors, also for the first time experimentally observed as will be presented later in this paper. The timescale of this fast adjustment is in experiments however much slower than predicted in simulations - on the timescale of minutes compared to seconds.

2. 10th turn pulsing

The 10th turn pulsing pattern was tested in 2016 with an excitation in the vertical plane only. In summary, the following experimental results were obtained:

1. Increase of the loss rate with the excitation amplitude as shown in Figs. 11 and ??.
2. Increase of the emittance growth with the excitation amplitude in the vertical plane but not in the horizontal plane shown in Fig. 11.
3. Change of the beam distribution due to the resonant excitation illustrated in Fig. 11 and 12.
4. As loss rates, emittance growth and distribution stayed unchanged for the 4 reference bunches, the

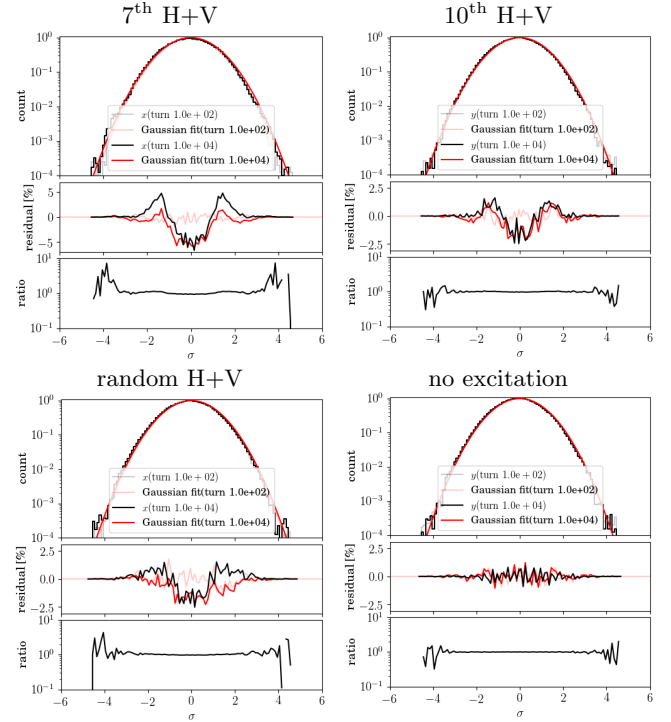


FIG. 10. Horizontal beam distribution for 7th turn pulsing (top left), vertical beam distribution for 10th turn pulsing (top right) and horizontal (bottom left) and vertical (bottom right) beam distribution for random excitation from Distribution Tracking simulations based on the 2016 injection optics with (Q_x, Q_y) = (64.28, 59.31) and standard errors. The excitation is applied in both planes with an amplitude of 96 nrad. The residual is defined as the final distribution (here 10⁴ turns) minus the initial distribution (here 10² turns), and the ratio as the final distribution divided by the initial distribution. The red line in the plot of the residual is the difference between the Gaussian fit of the distribution and the distribution itself.

above observations can be truly associated with the effect of the resonant excitation.

Besides the determination of the scaling of the loss rate and emittance growth with the excitation amplitude as required for the specification of the hollow electron lens, the most novel observation is the direct measurement of the change of the beam distribution, here with the Beam Synchrotron Radiation Telescope (BSRT) [23]. As an example for the change in distribution, the vertical profile of a reference bunch and one bunch experiencing the maximum excitation of $5 \cdot \Delta A = A_{\max}$ are compared in Fig. 12. The distribution of the excited bunch clearly changes and becomes non-Gaussian, while the reference bunch stays unchanged.

Comparing these experimental results with the simulations including only the excitation through the 10th turn pulsing and no random component and emittance growth only in the vertical plane (solid line in Fig. 13), the simulations predict qualitatively correctly an excitation amplitude dependent loss rate, but fail to predict the excita-

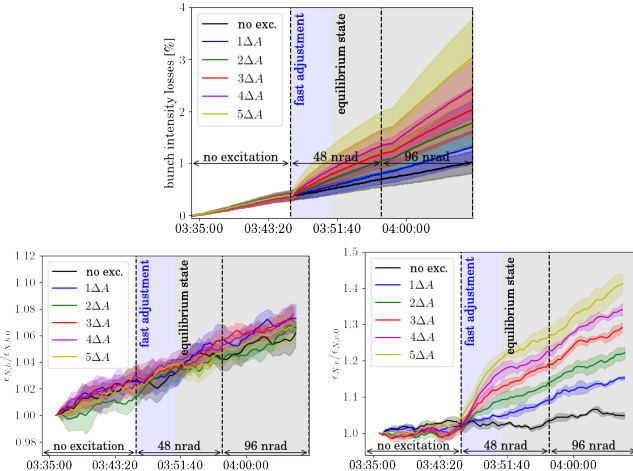


FIG. 11. Relative intensity (top) and relative emittance (bottom) averaged over the bunches experiencing the same excitation amplitude during the 2016 experiments. For each maximum amplitude $A_{\max} = 48$ nrad and 96 nrad, the excitation amplitude was linearly increased for each group of 4 bunches (see Sec. IV B). The different colored solid lines labeled with $n\Delta A$ indicate the average over the 4 bunches with the same excitation amplitude together with the 1σ standard deviation as their envelope.

tion amplitude dependent, continuous emittance growth observed in experiments. Instead, the simulations yield a constant emittance after an initial increase during the first 10^4 turns or first second. So obviously there is an essential ingredient missing. As it turns out, the constant emittance can be changed to an excitation amplitude dependent emittance growth by adding a random dipole noise component with uniform distribution representing the natural noise present in the LHC (dotted line in Fig. 13). As no noise estimate is available at injection for the LHC, a first estimate is obtained by scaling the estimate for 6.5 TeV [29, 30] by the magnetic rigidity to the injection energy of 450 GeV. This yields a maximum kick amplitude at the transverse damper of approximately

$$\theta_{\text{random,ADT,max}}(450 \text{ GeV}) = 6 \text{ nrad}, \quad (17)$$

Adding this random noise component, the simulations then yield correctly an excitation amplitude dependent emittance growth in the vertical plane after a first fast adjustment of the beam distribution visible as an increased initial value. Adding a random noise component has also the effect of increasing the loss rate. As the loss rates are in general underestimated in simulations compared to the experimental results, the discrepancy between simulations and experiment is therefore further reduced, but a large difference still prevails as illustrated in Fig. 14 by means of a qualitative comparison of the loss rates obtained in experiments and simulations.

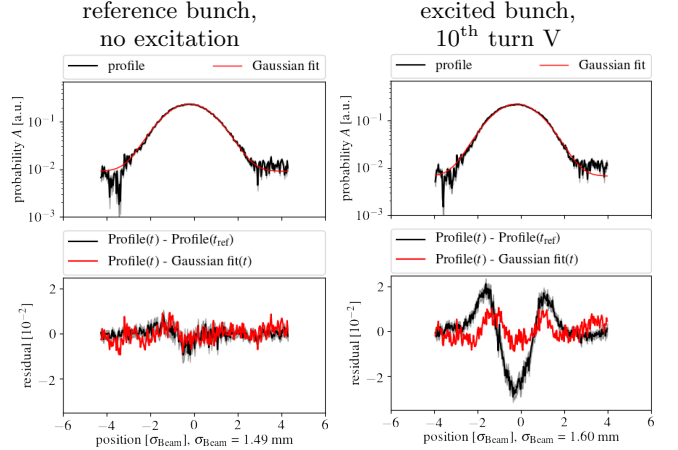


FIG. 12. Vertical beam profiles measured with the Beam Synchrotron Radiation Telescope (BSRT) during the 2016 experiments. The profiles are taken at the end of the 10th turn pulsing in V. For both bunches the transverse damper is not active. The black line in the plot of the residual is the current profile minus the profile before applying the excitation and is a measure for the overall change of the distribution. The red line is the current profile minus its Gaussian fit, which gives an indication for the deviation of the distribution from a Gaussian distribution. For details on the analysis see [23]. The distribution of the reference bunch (left), here slot 50, stays unchanged, while the bunch experiencing the maximum excitation (right), here slot 1300, clearly shows a change to a non-Gaussian distribution.

3. 7th turn pulsing

TABLE VI. Overview of the effect of 7th turn pulsing during the two resonant excitation experiments in 2016 [21] and 2017 [22]. The plane of the excitation is abbreviated with H for horizontal, V for vertical and H+V for horizontal and vertical at the same time.

Parameter	Experiment 2017	Experiment 2016
optics	2017 injection optics	2016 injection optics
tune (Q_x, Q_y)	(62.27, 60.295)	(64.28, 59.31)
excitation plane	H, V and H+V	H
losses	similar loss rates for pulsing in H, V and H+V	large losses for pulsing in H
hor. emit. growth	no	yes, very small
vert. emit. growth	yes, for pulsing in V and H+V	no

The 7th turn pulsing pattern has been tested during both experiments in 2016 and 2017 and was intended to serve as a proof for the reproducibility of the results. However, in 2017 the machine tune was changed from (64.28, 59.31) to (62.27, 60.295) in standard operation accompanied by a slight change in optics. The attempt to change back to the fractional tune of (.28,.31) as chosen in 2016 lead to large losses during the experiment in 2017 and therefore the 2017 working point of

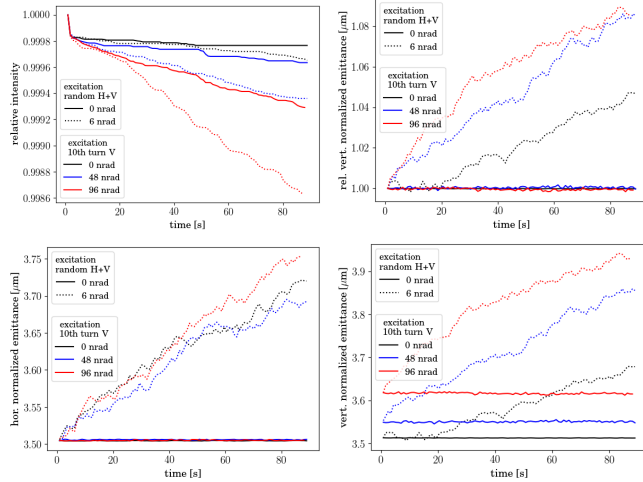


FIG. 13. Relative intensity (top left) and relative vert. emittance (top right), and hor. (bottom left) and vert. (bottom right) emittance obtained from simulations (Distribution Tracking) based on the 2016 injection optics with standard errors and $(Q_x, Q_y) = (64.28, 59.31)$. The solid line indicates an excitation with only 10th turn pulsing in V and the dotted line with 10th turn pulsing in V plus a random dipole noise component in H+V of 6 nrad.

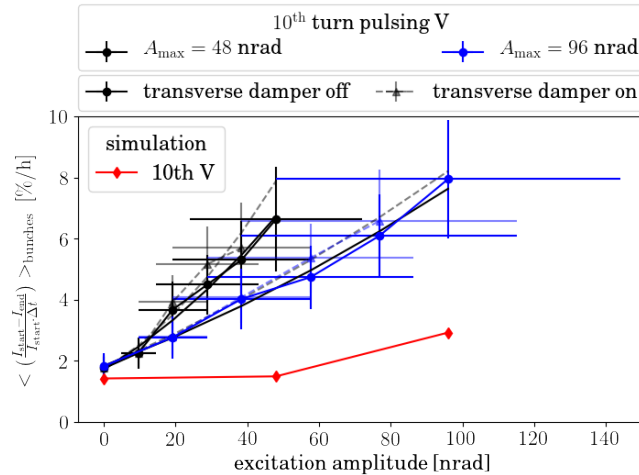


FIG. 14. Comparison of scaling of loss rates with excitation amplitude for 10th turn pulsing. The experimental results are shown in black (maximum excitation with 48 nrad) and blue (maximum excitation with 96 nrad). The excitation amplitude error is 50% due to limited measurement accuracy and the error on the loss rate is the pure statistical error. The simulation results (2016 injection optics, standard errors, $(Q_x, Q_y) = (64.28, 59.31)$, 10th turn pulsing in V plus random dipole noise in H+V of 6 nrad) are shown in red.

(62.27,60.295) was used instead. This change in tune entailed a change in the driving resonances, from previously the $7Q_x$ resonances in 2016 (Fig. 9) to the $7Q_x$, $7Q_y$ and $7Q_x + 7Q_y$ resonance in 2017 (Fig. 15). Consequently, the effects on the beam also differ as can be illustrated by a comparison of the Distribution Tracking for both

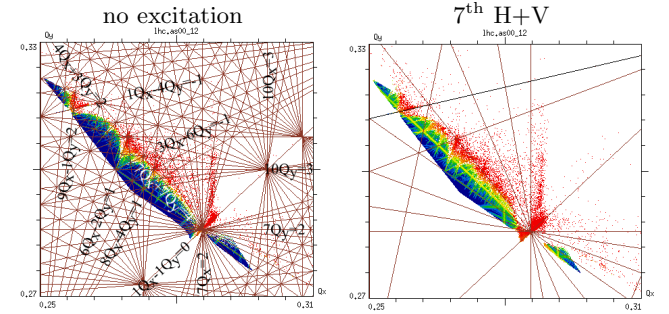


FIG. 15. FMA analysis in frequency space for 7th turn pulsing based on the 2017 injection optics with no machine errors and a tune of (62.27,60.295). The excitation is 96 nrad in both planes. The $7Q_x$ and $7Q_y$ resonance are both excited and in addition the 14th order $7Q_x + 7Q_y$.

experiments (Fig. 16).

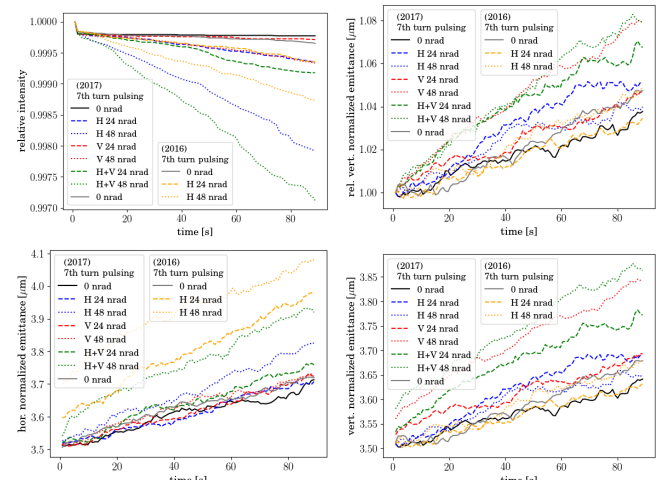


FIG. 16. Relative intensity (top left) and relative vert. emittance (top right), and hor. (bottom left) and vert. (bottom right) emittance obtained from simulations (Distribution Tracking) based on the 2016 injection optics with standard errors and $(Q_x, Q_y) = (64.28, 59.31)$ and 2017 injection optics with standard errors and $(Q_x, Q_y) = (62.27, 60.295)$. The solid line indicates an excitation with only a random dipole noise component in H+V of 6 nrad, and the dotted and dashed line the results for 7th turn pulsing plus a random dipole noise component in H+V of 6 nrad.

Similar changes of the emittance are also experimentally observed as shown in Fig. 17, where emittance growth was observed only in the horizontal plane for 2016 for pulsing in H, and only in the vertical plane for 2017 for pulsing in V and H+V (for pulsing in H no emittance growth is observed). Just as for the 10th turn pulsing (Fig. 11), the emittance growth can be divided also for the 7th turn pulsing in a phase of fast adjustment of the beam distribution and the reach of a new equilibrium state (Fig. 17). Also in this case, the distribution changes are also directly visible on the beam profiles measured

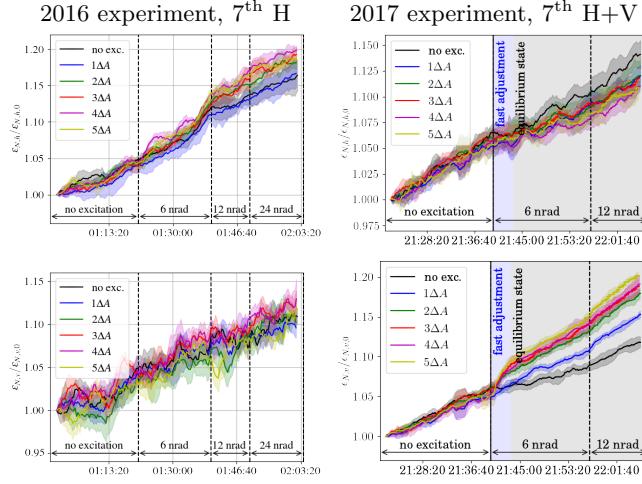


FIG. 17. Relative horizontal (top) and vertical (bottom) emittance obtained during the 2016 experiments (left) and the 2017 experiment (right) averaged over the bunches experiencing the same excitation amplitude.

with the BSRT (Appendix B, Fig. 29).

The loss rates measured during the experiment however differ from the simulations in terms of for which case the largest rate is observed as well as quantitatively for the specific cases. For example smaller losses are expected for the 2016 experiments compared to the 2017 experiments from simulations, while experimentally higher loss rates were measured in 2016 (Fig. 18).

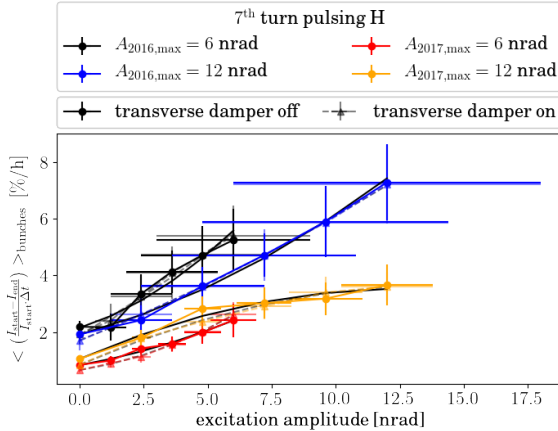


FIG. 18. Comparison of scaling of loss rates with excitation amplitude for 7th turn pulsing in H and data obtained during the 2016 experiment (black and blue) and 2017 experiment (red and yellow). The excitation amplitude error is 50% in 2016 and could be reduced to 15% in 2017.

4. 8th turn pulsing

Pulsing patterns which have little effect on the beam core are particularly interesting for the hollow electron

lens operation if they on the other hand have a large effect on the tails under consideration of the non-linear field generated by the electron lens itself. With this motivation in mind the 8th turn pulsing pattern was studied, for which a small effect is expected in comparison to the 7th and 10th turn pulsing as can be demonstrated in the Distribution Tracking, for which the excitation amplitudes had to be increased to 96 nrad to have a visible effect (Fig. 19). The loss rates and also changes in bunch length are very small and any differences are here just due to statistical fluctuations. In the horizontal and vertical plane a small emittance growth due to the excitation is visible, but without any clear dependency on the amplitude nor plane of the 8th turn pulsing. Adducting the FMA analysis in amplitude space depicted in Fig. 20, the 8th turn pulsing drives the $16Q_y$ and $8Q_x - 4Q_y$ resonances and several even higher orders. These are in general very high order resonances whose effect is thus in general expected to be small.

The only small effect on the beam expected from simulations could then be also confirmed experimentally during the 2017 experiments. For this purpose the excitation amplitude was increased to 96 nrad, which is the maximum kick strength reachable with the transverse damper at injection without risking saturation. As depicted in Fig. 21, the loss rate increased slightly with the excitation amplitude for an excitation in H+V. For an excitation only in V or only in H, no statistically relevant increase was observed. In addition, the beam distribution also changed in the horizontal plane for an excitation only in H as visible in the BSRT profiles (Appendix B, Fig. 30)

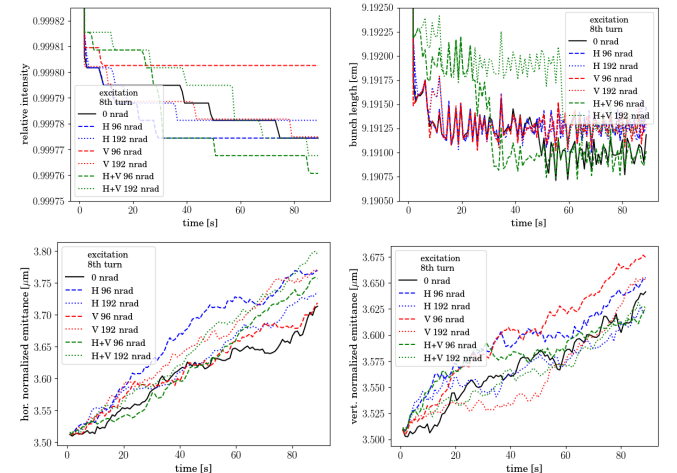


FIG. 19. Relative intensity (top left), bunch length (top right), and horizontal (bottom left) and vertical (bottom right) emittance obtained from simulations (Distribution Tracking) based on the 2017 injection optics with standard errors and $(Q_x, Q_y) = (62.27, 60.295)$. The solid line indicates an excitation with only a random dipole noise component in H+V of 6 nrad, and the dotted and dashed line the results for 8th turn pulsing plus a random dipole noise component in H+V of 6 nrad.

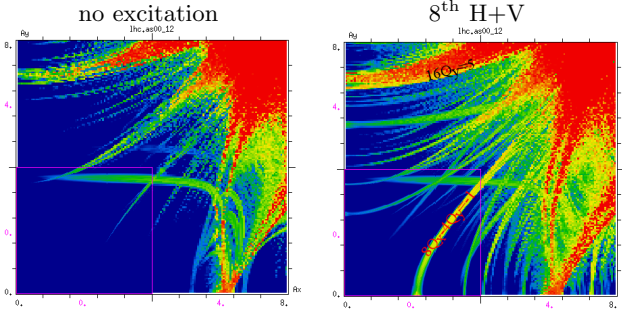


FIG. 20. FMA analysis in amplitude space for 8th turn pulsing based on the 2017 injection optics with no machine errors and a tune of (62.27,60.295). The excitation is 96 nrad in both planes. The $16Q_y$ and $8Q_x - 4Q_y$ are both excited.

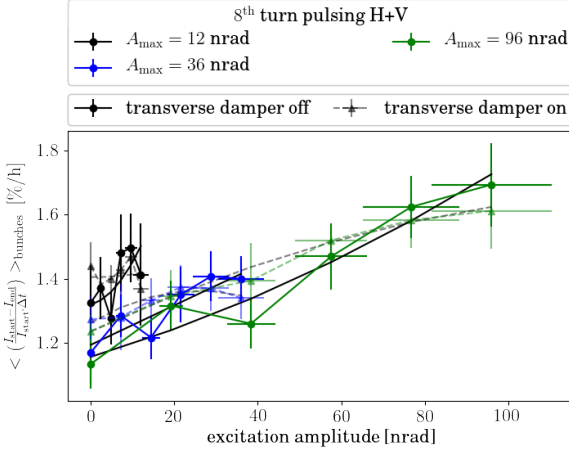


FIG. 21. Comparison of scaling of loss rates with excitation amplitude for 8th turn pulsing in H+V measured during the 2017 experiment. The excitation amplitude error is 15% indicated by the horizontal error bars.

indicating an increase at around 2.0σ simultaneously with a depletion of the beam core. For an excitation in H+V the emittances of the references bunches were much smaller, around $1.8\mu\text{m}$ normalized emittance on average, than the one of the excited bunches ranging from $2.3\mu\text{m}$ to $3.0\mu\text{m}$ [22]. The references bunches thus experienced a stronger emittance growth due to intra-beam scattering than the excited bunches due to the excitation on top of their smaller emittance growth due to intra-beam scattering.

5. random excitation

In view of the electron lens, the random excitation presents the pulsing pattern leading to the fastest halo depletion rates. On the other hand it also represents the most dangerous pattern for the beam core. The aim of this experiment was to test the effect on the beam core in comparison to the resonant excitation represented in the 2017 experiment by the 7th turn pulsing as for 8th turn

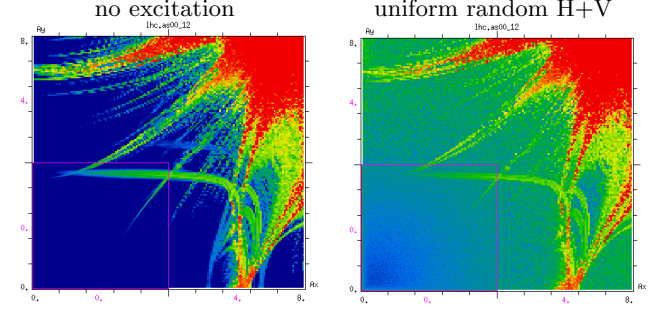


FIG. 22. FMA analysis in amplitude space for a uniform random excitation with 1 nrad amplitude in H+V based on the 2017 injection optics with no machine errors and a tune of (62.27,60.295). The diffusion in tune is increased equally independent of the amplitude.

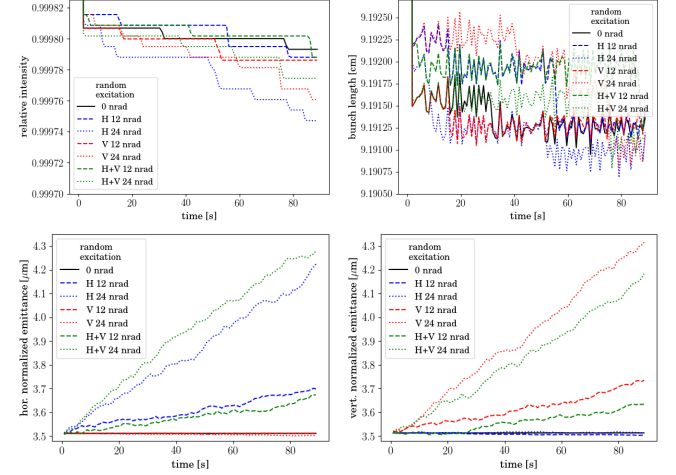


FIG. 23. Relative intensity (top left), bunch length (top right), and horizontal (bottom left) and vertical (bottom right) emittance obtained from simulations (Distribution Tracking) based on the 2017 injection optics with standard errors and $(Q_x, Q_y) = (62.27, 60.295)$. The solid line indicates the case with no excitation, and the dotted and dashed line the results for a uniform random excitation of 12 nrad and 24 nrad respectively.

pulsing basically no effect was observed. The random excitation is so powerful in cleaning the halo as it excites all frequencies equally. This can be seen formidably with the FMA analysis in amplitude space depicted in Fig. 22. The diffusion in tune is increased equally independent of the amplitude.

The results from the Distribution Tracking are shown in Fig. 23. In contrast to the 7th and 10th turn pulsing, the effect of a random excitation is very symmetric:

- Emittance growth is only caused in the plane of excitation.
- The emittance growth is comparable between an excitation in H and V in the corresponding plane as well as the scaling with the excitation amplitude. Only a small increase or decrease is observed if the

excitation is applied in both planes. The difference can be attributed to coupling.

- The random excitation leads to an increased constant emittance growth rate which is reached without undergoing an initial adjustment phase.
- Negligible losses are observed independent of the plane of excitation.

Qualitatively, this behavior could be also confirmed experimentally during the 2017 experiments and as example the emittances are depicted in Fig. 24 for pulsing in V and in H+V, showing no emittance growth in the horizontal for an excitation only in V and emittance growth in both planes for an excitation in H+V. All emittance growth rates are in a comparable range. Note that despite the large emittance growth, the growth rate stays constant and there is no fast adjustment phase succeeded by a new equilibrium state as was the case for the 7th and 10th turn pulsing. These large changes of the emittance

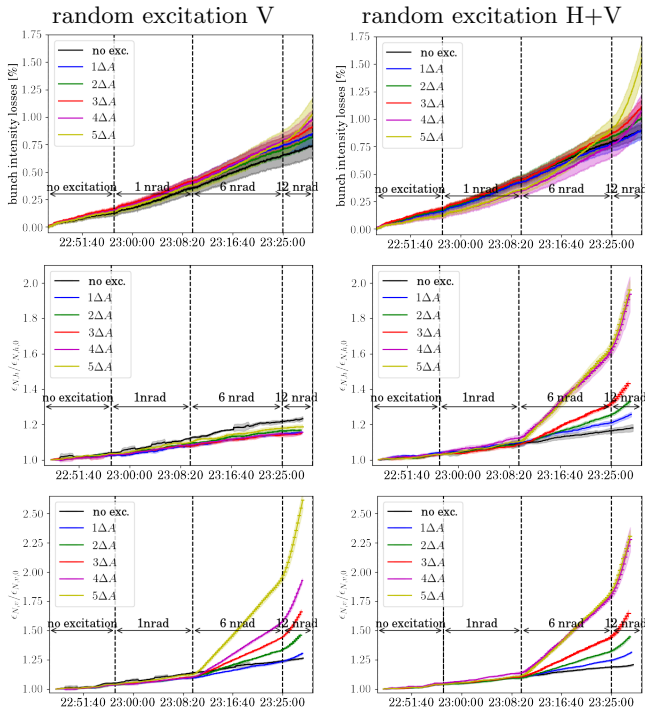


FIG. 24. Relative intensity (top) and relative horizontal (center) and vertical (bottom) emittance for a random excitation only in V (left) and in H+V (right). Emittance growth is only caused in the plane of excitation.

can of course also be seen directly in the BSRT profiles shown in Fig. 25 for a random excitation only in V. In comparison to for example the 10th turn pulsing (Fig. 12), the distribution also stays Gaussian in case of a random excitation while for the 10th turn pulsing it clearly adopts a non-Gaussian shape.

The experimental results also confirm the small loss predicted in simulations. The losses then suddenly increase for 12 nrad, which is most likely the point when,

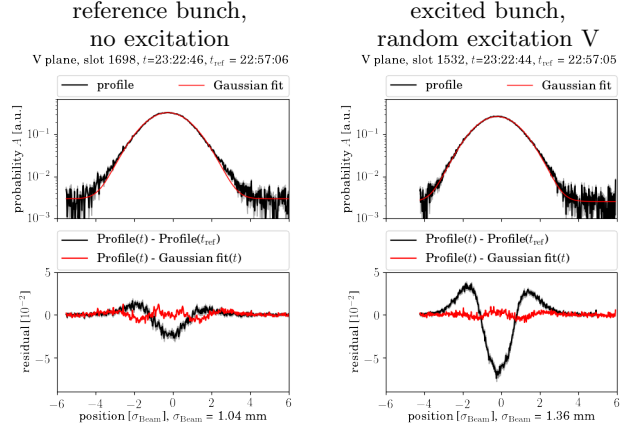


FIG. 25. Vertical beam profiles measured with the Beam Synchrotron Radiation Telescope (BSRT) during the 2017 experiments. The profiles are taken at the end of the random excitation in V, here slot 1698, are much less than for the bunch experiencing the maximum excitation (right), here slot 2696.

due to the large emittance increase, the physical aperture starts eating into the more central region of the distribution causing higher losses. Furthermore, the loss rates also add up, meaning that double the loss rate is observed for an excitation in H+V compared to only in H or only V. This is illustrated in Fig. 26, which also shows the loss rates for the 7th turn pulsing in comparison. Furthermore the loss rate is considerably reduced if the transverse damper is active, which is not the case for the 7th turn pulsing. We will address this subject separately in the next Section, Sec. IV D 6.

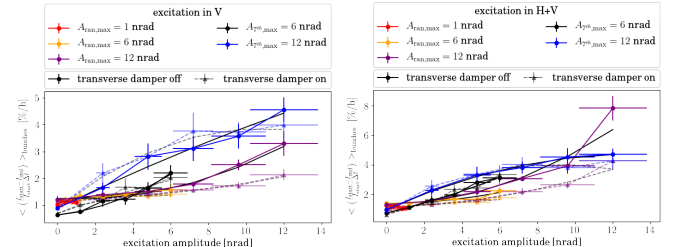


FIG. 26. Comparison of scaling of loss rates with excitation amplitude for a random excitation and 7th turn pulsing in V (left) and H+V (right) measured during the 2017 experiment. The excitation amplitude error is 15% indicated by the horizontal error bars. Note that for 7th turn pulsing the transverse damper does not influence the loss rate, while for a random excitation the loss rate is considerably reduced for the bunches with transverse damper active.

6. Effect of the transverse damper

For all k^{th} turn pulsing patterns, the transverse damper does not change any of the observables studied during the experiments, explicitly losses, emittance and beam distribution suggesting that indeed it is not capable of damping any resonant excitation. On the other hand, the transverse damper considerably decreases loss rates, emittance growth and distribution changes for the random excitation. As an example, the vertical emittance growth is compared for the 7th turn pulsing in V and a random excitation in V in Fig. 27 and the loss rates in Fig. 26 illustrating impressively the above behavior. For nth turn pulsing no effect. Show example of emittance for 7th turn pulsing and random and refer to Fig. 26 for the loss rate. Any idea why? Daniel, help!

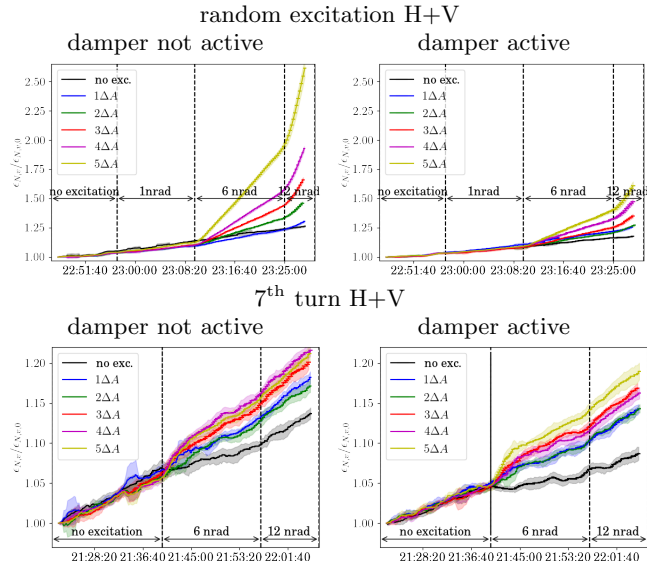


FIG. 27. Relative intensity for bunches with transverse damper not active (top) and transverse damper active (bottom) for 7th turn pulsing in V (left) and for a random excitation only in V (right).

V. SUMMARY

We now want to close the loop to the effects on the beam core for hollow electron lenses in HL-LHC. For DC operation, no influence on the beam core are to be expected. To study the effect of pulsed operation beam experiments were conducted in 2016 and 2017 at injection. The experimental results showed that for the kick amplitudes expected for the e-lens, considerable effects are to be expected. The random pulsing mode is the most sensitive pulsing pattern and as it excites all beam frequencies results in emittance growth in the plane of excitation and losses once the beam size increased enough to hit the physical aperture. The resonant excitation or nth turn pulsing on the other hand features a rich non-linear dy-

namics as it excites only certain resonances and diversity in beam distribution and diffusion changes. This means, that each pulsing patterns results in different loss rates and emittance growth. Typical for this kind of excitation is also the adjustment of the beam distribution to a new equilibrium state.

ACKNOWLEDGMENTS

We wish to acknowledge Giulia Papotti with her help with the preparations for the 2016 experiments and her general support from the operations side, Roderik Bruce and Gianluca Valentino for their very helpful suggestions in preparing the experiment at the LHC and we would like to thank all participants of the experiment for helping acquire the data presented in this paper. We would like to acknowledge Dmitry Shatilov for his help with the Lifetrac code, and Stéphane Fartoukh, Riccardo De Maria and Rogelio Toms for their help with generating the appropriate optics model. We are grateful also for the support from the beam instrumentation team, in particular Enrico Bravin and Georges Trad, with the BSRT and are thankful for the collaboration with Stéphanie Papadopoulou and Fanouria Antonio for the analysis of the BSRT profiles.

Appendix A: FMA analysis for 10th turn pulsing and 2016 optics and tune

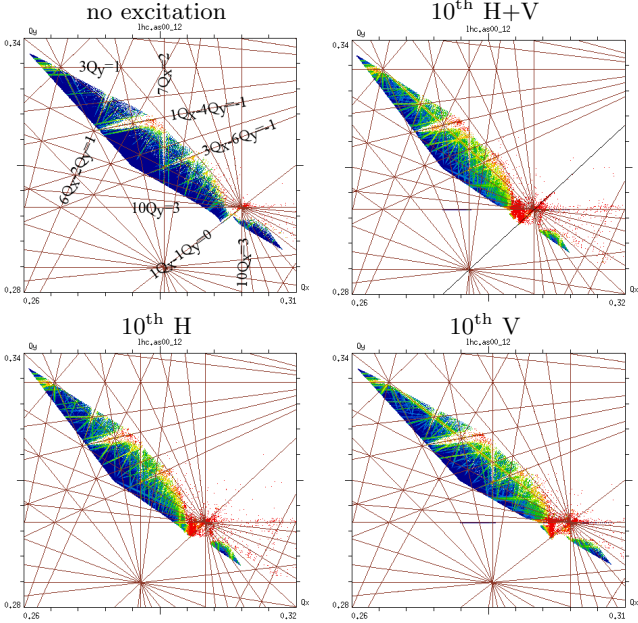


FIG. 28. FMA analysis for 10th turn pulsing based on the 2016 injection optics with no machine errors and a tune of (64.28,59.31). The excitation is 120 nrad in the corresponding plane. There is no significant difference in the FMA analysis between pulsing only in H, only in V or in H+V.

Appendix B: BSRT profiles for 7th and 8th turn pulsing during 2017 experiments

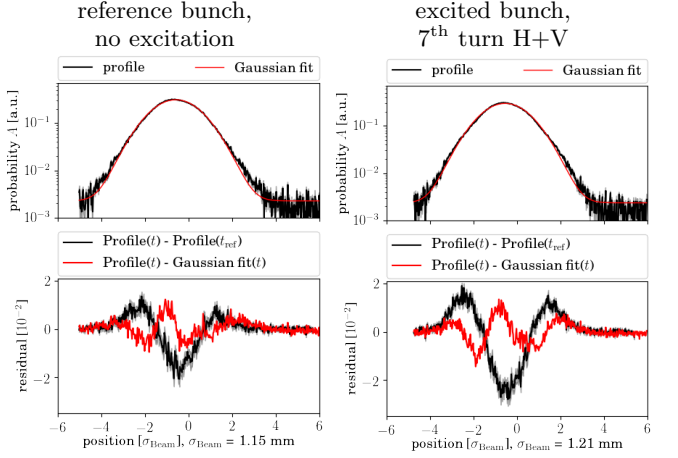


FIG. 29. Vertical beam profiles measured with the Beam Synchrotron Radiation Telescope (BSRT) during the 2017 experiments. The profiles are taken at the end of the 7th turn pulsing in H+V. For both bunches the transverse damper is not active. The distribution changes in the reference bunch (left), here slot 2862, are much less than for the bunch experiencing the maximum excitation (right), here slot 2696.

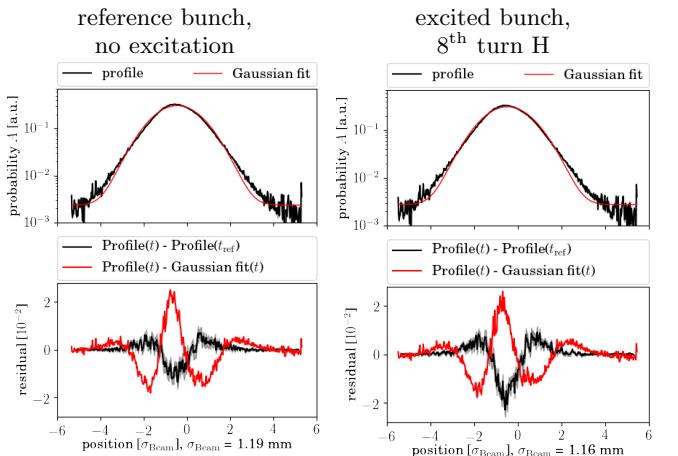


FIG. 30. Horizontal beam profiles measured with the Beam Synchrotron Radiation Telescope (BSRT) during the 2017 experiments. The profiles are taken at the end of the 8th turn pulsing in H. For both bunches the transverse damper is not active. The distribution changes in the reference bunch (left), here slot 804, are much less than for the bunch experiencing the maximum excitation (right), here slot 632.

-
- [1] S. Holmes, R. S. Moore, and V. Shiltsev, *Journal of Instrumentation* **6**, T08001 (2011).
- [2] D. Nisbet, “2016 operation: Operational efficiency and lessons learnt,” (2017), LHC Performance Workshop 2017.
- [3] O. S. Brüning, P. Collier, P. Lebrun, S. Myers, R. Ostojic, J. Poole, and P. Proudlock, *LHC Design Report*, CERN Yellow Reports: Monographs (CERN, Geneva, 2004).
- [4] A. G., B. A. I., B. O., F. P., L. M., R. L., and T. L., *High-Luminosity Large Hadron Collider (HL-LHC): Technical Design Report V. 0.1*, CERN Yellow Reports: Monographs (CERN, Geneva, 2017).
- [5] M. Benedikt and F. Zimmermann, *Future Circular Colliders*, Tech. Rep. CERN-ACC-2015-0164 (CERN, Geneva, 2015).
- [6] G. Valentino, “What did we learn about halo population during MDs and regular operation?” (2016), Review of the needs for a hollow e-lens for the HL-LHC.
- [7] “Review on the needs for a hollow e-lens for the HL-LHC,” (2016).
- [8] R. Bruce, “Alternative methods for halo depletion (damper, tune modulation, and wire), long range beam-beam and comparison of their performance/reliability to that of a hollow electron lens.” (2016), review of the needs for a hollow e-lens for the HL-LHC.
- [9] *Proceedings, EuCARD-AccNet-EuroLumi Workshop: The High-Energy Large Hadron Collider (HE-LHC10): Villa Bighi, Malta, Republic of Malta, October 14-16, 2010* (2011) arXiv:1108.1617 [physics.acc-ph].
- [10] J. Molson, R. Bruce, A. Faus-Golfe, M. Fiascaris, A. Krainer, and S. Redaelli, in *Proceedings, 8th International Particle Accelerator Conference (IPAC 2017): Copenhagen, Denmark, May 14-19, 2017* (2017) p. MOPAB001.
- [11] G. Stancari, A. Valishev, G. Annala, G. Kuznetsov, V. Shiltsev, D. A. Still, and L. G. Vorobiev, *Phys. Rev. Lett.* **107**, 084802 (2011).
- [12] X.-L. Zhang, K. Bishopberger, V. Kamerdzhev, V. Lebedev, V. Shiltsev, R. Thurman-Keup, and A. Tollestrup, *Phys. Rev. ST Accel. Beams* **11**, 051002 (2008).
- [13] G. Stancari, V. Previtali, A. Valishev, R. Bruce, S. Redaelli, A. Rossi, and B. S. Ferrando, *Conceptual design of hollow electron lenses for beam halo control in the Large Hadron Collider*, Tech. Rep. FERMILAB-TM-2572-APC, CERN-ACC-2014-0248 (Fermilab, CERN, 2014) arXiv:1405.2033 [physics.acc-ph].
- [14] G. Stancari, *Calculation of the Transverse Kicks Generated by the Bends of a Hollow Electron Lens*, Tech. Rep. FERMILAB-FN-0972-APC (Fermilab, 2014) arXiv:1403.6370 [physics.acc-ph].
- [15] I. A. Morozov, G. Stancari, A. Valishev, and D. N. Shatilov, *Proceedings, 3rd International Conference on Particle accelerator (IPAC 2012): New Orleans, USA, May 2-25, 2012*, Conf. Proc. IPAC 2012 **C1205201**, 94 (2012).
- [16] “Hl-lhc optics v1.3,” LHC optics web.
- [17] M. Fitterer, G. Stancari, and A. Valishev, *Effect of pulsed hollow electron-lens operation on the proton beam core in LHC*, Tech. Rep. FERMILAB-TM-2635-AD (Fermilab, 2016).
- [18] “Electron lens test stand.”
- [19] G. Stancari, “Electron-beam simulations: electron-gun emission and residual fields from measured profiles,” HEL Electron Beam results discussion.
- [20] “The warp code.”
- [21] M. Fitterer, G. Stancari, A. Valishev, R. Bruce, P. S. Papadopoulou, G. Papotti, D. Pellegrini, S. Redaelli, G. Trad, D. Valuch, G. Valentino, J. Wagner, and C. Xu, (2016).
- [22] M. Fitterer, G. Stancari, A. Valishev, R. Bruce, P. S. Papadopoulou, G. Papotti, D. Pellegrini, S. Redaelli, G. Trad, D. Valuch, G. Valentino, J. Wagner, and C. Xu, (2018).
- [23] M. Fitterer and G. Stancari, *Analysis of BSRT profiles in the LHC at injection*, Tech. Rep. FERMILAB-TM-2657-AD-APC (Fermilab, 2017).
- [24] T. Linnecar, M. E. Angloetta, L. Arnaudon, P. Baudrenghien, T. Bohl, O. Brunner, A. Butterworth, E. Ciapala, F. Dubouchet, J. Ferreira-Bento, D. Glenat, G. Hagmann, W. Hfle, C. Julie, F. Killing, G. Kotzian, D. Landre, R. Louwense, P. Maesen, P. Martinez-Yanez, J. Molendijk, E. Montesinos, C. Nicou, J. Noirjean, G. Papotti, A. Pashnin, G. Pechaud, J. Pradier, V. Rossi, J. Sanchez-Quesada, M. Schokker, E. Shaposhnikova, R. Sorokoletev, D. Stellfeld, J. Tckmantel, D. Valuch, U. Wehrle, and F. Weierud, *Hardware and Initial Beam Commissioning of the LHC RF Systems*, Tech. Rep. LHC-PROJECT-Report-1172. CERN-LHC-PROJECT-Report-1172 (CERN, Geneva, 2008).
- [25] W. Höfle, G. Kotzian, M. Schokker, and D. Valuch, “LHC Damper Beam commissioning in 2010,” (2011).
- [26] X. Buffat, J. Barranco Garcia, T. Pieloni, C. Tambasco, and D. Valuch, Conf. Proc. IPAC 2017 (2017).
- [27] J. Laskar, *Particle accelerator. Proceedings, Conference, PAC 2003, Portland, USA, May 12-16, 2003*, Conf. Proc. **C030512**, 378 (2003).
- [28] D. Shatilov, Y. Alexahin, V. Lebedev, and A. Valishev, *Particle accelerator. Proceedings, Conference, PAC'05, Knoxville, USA, May 16-20, 2005*, Conf. Proc. PAC'05 (2005).
- [29] X. Buffat, N. Biancacci, S. V. Furuseth, D. Jacquet, E. Metral, D. Pellegrini, M. Pojer, G. Trad, D. Valuch, J. Barranco Garcia, T. Pieloni, C. Tambasco, and Q. Li, (2017).
- [30] J. Barranco Garcia, X. Buffat, T. Pieloni, C. Tambasco, G. Trad, D. Valuch, M. Betz, M. Wendt, M. Pojer, M. Solfaroli Camillocci, B. M. Salvachua Ferrando, K. Fuchsberger, M. Albert, and J. Qiang, *MD 400: LHC emittance growth in presence of an external source of noise during collision*, Tech. Rep. CERN-ACC-NOTE-2016-0020 (CERN, 2016).